Supporting Information

Piranha Solution-Assisted Surface Engineering Enables Silicon Nanocrystals with Superior Wettability and Lithium Storage

Tingting Li, Yangfan Li, Fan Zhang, Naiwen Liang, Jiang Yin, Haihong Zhao,*
Yahui Yang, Bo Chen,* Lishan Yang*

National and Local Joint Engineering Laboratory for New Petrochemical Materials and Fine Utilization of Resources, Key Laboratory of the Assembly and Application of Organic Functional Molecules of Hunan Province, Hunan Normal University, Changsha, 410081, P.R. China.
State Key Laboratory of Organic Electronics and Information Displays & Jiangsu Key Laboratory for Biosensors, Institute of Advanced Materials (IAM), School of Chemistry and Life Sciences, Nanjing University of Posts and Telecommunications, Nanjing, 210023, P. R. China.
E-mail: zhh_1998@163.com (Haihong Zhao); iambchen@njupt.edu.cn (Bo Chen); lsyang@hunnu.edu.cn (Lishan Yang).
Tel./Fax.: +86 731-88872531 (Lishan Yang).

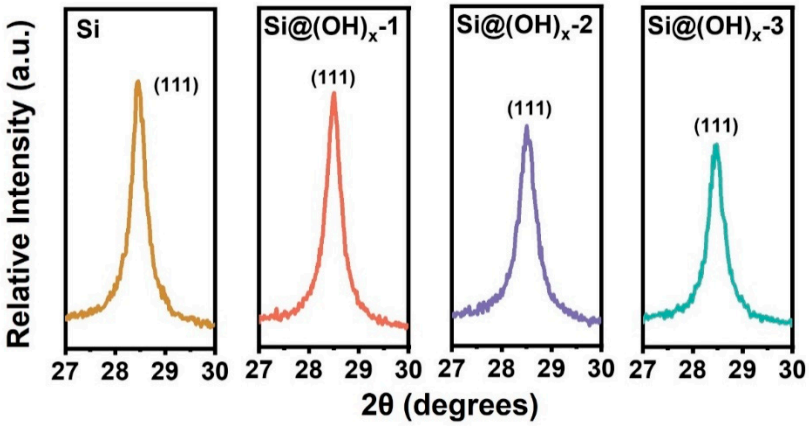

Figure S1. Partial enlargement of XRD patterns of Si, Si@Si(OH)$_x$-1, Si@Si(OH)$_x$-2, and Si@Si(OH)$_x$-3 nanoparticles.

Table S1. Calculated particles sizes of Si, Si@Si(OH)$_x$-1, Si@Si(OH)$_x$-2, and Si@Si(OH)$_x$-3 based on the Scherrer formula.

Material	D (nm)
Si	16.74
Si@Si(OH)x-1	16.43
Si@Si(OH)x-2	14.74
Si@Si(OH)x-3	16.12

Scherrer formula: $D=\frac{K\lambda}{\beta COS\theta}$

D: diameter of crystals (nm)
K: scherrer constant (take 0.89)
λ: X-ray wavelength (take 0.15406 nm)
β: FWHM
θ: diffraction angle

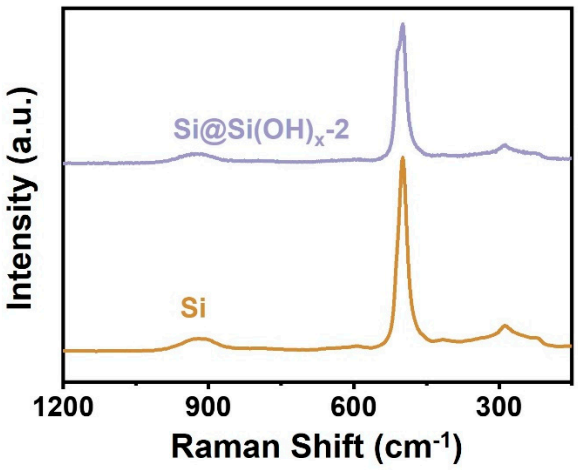

Figure S2. Raman spectra of Si and Si@Si(OH)$_x$-2.

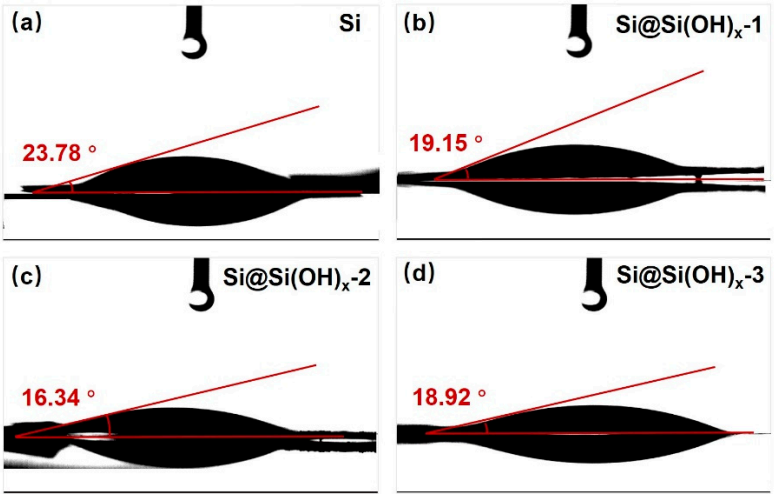

Figure S3. Photos of Si, Si@Si(OH)$_x$-1, Si@Si(OH)$_x$-2, and Si@Si(OH)$_x$-3 electrodes after contact angle tests.

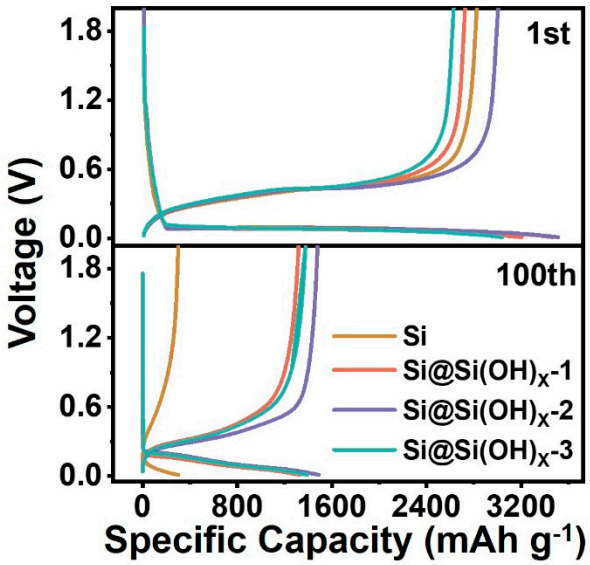

Figure S4. The charge-discharge profiles of Si, Si@Si(OH)$_x$-1, Si@Si(OH)$_x$-2, and Si@Si(OH)$_x$-3 anodes at 1st and 100th cycles.

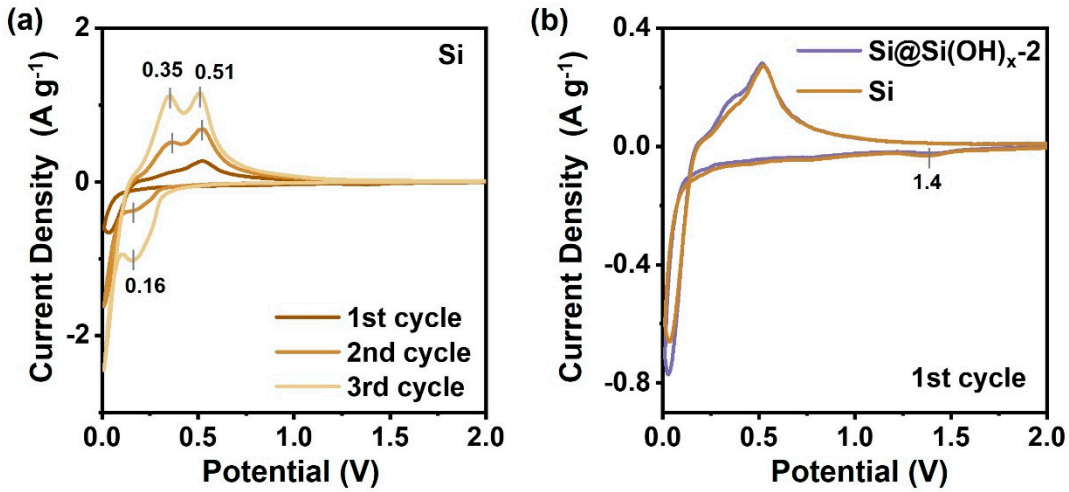

Figure S5. CV curves of (a) the Si anode and (b) the Si and Si@Si(OH)$_x$-2 anode for 1st cycle at a scan rate of 0.1 mV s^{-1}.

Table S2. The anodic performances comparison of different surface treatment methods.

Material	Pretreatment	Postprocessing	Binder	Initial capacity (mA h g^{-1})	Cycling performance	Current density (mA g^{-1})	Ref.
Si	pretreated in piranha solution (H_2SO_4/H_2O_2 = 3:1 v/v) at 65 °C for 2 h	---	SA	3095.5	924.3 mA h g^{-1} after 200 cycles	1000	This work
Si	pretreated in piranha solution (H_2SO_4/H_2O_2 = 3:1 v/v) at 80 °C for 2 h	---	SA	3394.7	1121.5 mA h g^{-1} after 200 cycles	1000	This work
Si	pretreated in piranha solution (H_2SO_4/H_2O_2 = 3:1 v/v) at 95°C for 2 h	---	SA	2935.0	992.3 mA h g^{-1} after 200 cycles	1000	This work
Si	pretreated in piranha solution (H_2SO_4/H_2O_2 = 3:1 v/v) at 85 °C for 1 h	---	PAA	3300	335 mA h g^{-1} after 50 cycles	1000	1
Si-MPs	treated in piranha solution (H_2SO_4/H_2O_2 = 3:1 v/v) at 85 °C for 1-2 h	---	PAA	3420	600 mA h g^{-1} after 50 cycles	1000	2
Si	stirred magnetically in piranha solution (H_2SO_4/H_2O_2 = 7:3 v/v) for 2 h at 80 °C	---	SA	2720	750 mA h g^{-1} after 50 cycles	2000	3
Si	modified by piranha solution (H_2SO_4/H_2O_2 = 3:1 v/v)	Coated by Graphene oxide composite	CMC, MTI	2737	1,563 mA h g^{-1} after 100 cycles	0.5 C	4
Si	modified by HCl piranha solution (H_2SO_4/H_2O_2 = 1:4 v/v) for 0.5 h at 85 °C	---	PAA	2907	737.3 mA h g^{-1} after 150 cycles	200	5

Table S3. The fitting data of the Si, Si@Si(OH)$_x$-1, Si@Si(OH)$_x$-2, and Si@Si(OH)$_x$-3 anodes.

Materials	Cycle	R_{ct} (Ω) / error %	Z_w-R (Ω) / error %	R_{sei} (Ω) / error %	Open circuit potential (V)
Si	Before	569/6	799/19	---	3.03
Si@Si(OH)$_x$-1	Before	530/3	629/22	---	3.08
Si@Si(OH)$_x$-2	Before	404/3	471/15	---	3.09
Si@Si(OH)$_x$-3	Before	554/3	669/17	---	3.05
Si	200th	1041/7	1173/12	81/2	0.42
Si@Si(OH)$_x$-1	200th	871/14	821/14	77/3	0.42
Si@Si(OH)$_x$-2	200th	830/8	697/12	70/5	0.42
Si@Si(OH)$_x$-3	200th	854/16	946/7	73/6	0.45

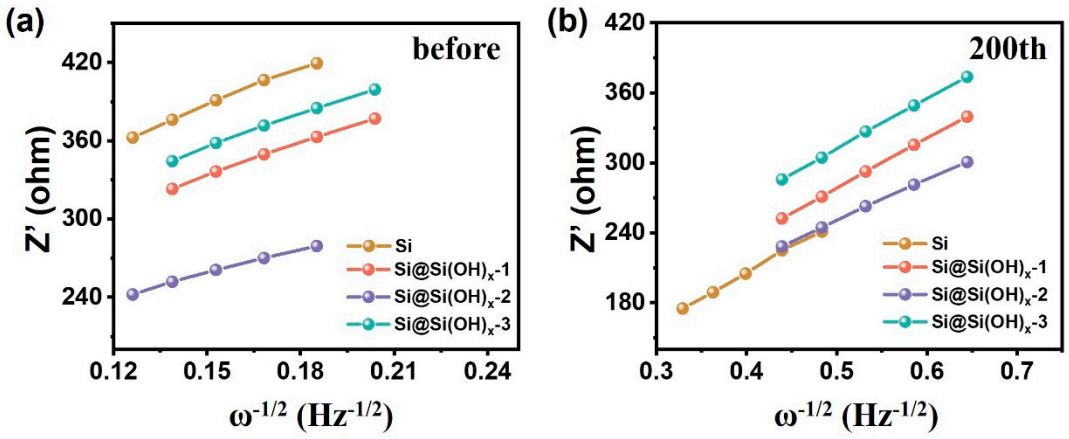

Figure S6. Z'~ $\omega^{-1/2}$ linear relationship diagram of (a) before cycling and (b) after 200 cycles.

Table S4. The fitting Warburg parameters of the Si, Si@$Si(OH)_x$-1, Si@$Si(OH)_x$-2, and Si@$Si(OH)_x$-3 anodes.

Materials	Cycle	σ
Si	Before	976.20
Si@$Si(OH)_x$-1	Before	825.48
Si@$Si(OH)_x$-2	Before	624.51
Si@$Si(OH)_x$-3	Before	840.05
Si	200th	435.59
Si@$Si(OH)_x$-1	200th	426.80
Si@$Si(OH)_x$-2	200th	353.44
Si@$Si(OH)_x$-3	200th	429.47

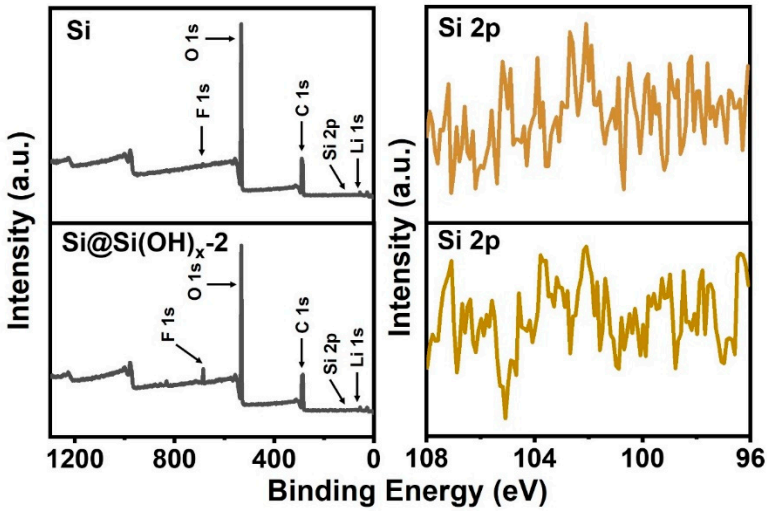

Figure S7. XPS spectra of the Si and Si@Si(OH)$_x$-2 electrode after 200 cycles.

References

1. Jung, C. H.; Kim, K. H.; Hong, S. H. Stable silicon anode for lithium-ion batteries through covalent bond formation with a binder via esterification. *ACS Appl. Mater. Interfaces* **2019**, *11*, 26753–26763.
2. Jung, C. H.; Kim, K. H.; Hong, S. H. An in situ formed graphene oxide-polyacrylic acid composite cage on silicon microparticles for lithium ion batteries via esterification reaction. *J. Mater. Chem. A* **2019**, *7*, 12763-12772.
3. Guo, S. T.; Li, H.; Li, Y. Q.; Han, Y.; Chen, K.; Xu, G. Z.; Zhu, Y. J.; Hu, X. L. SiO2-enhanced structural stability and strong adhesion with a new binder of konjac glucomannan enables stable cycling of silicon anodes for lithium-ion batteries. *Adv. Energy Mater.* **2018**, *8*, 1800434,
4. Cen, Y. J.; Qin, Q. W.; Sisson, R. D.; Liang, J. Y. Effect of particle size and surface treatment on Si/graphene nanocomposite lithium-ion battery anodes. *Electrochim. Acta* **2017**, *251*, 690–698,
5. Li, C.; Shi, T. F.; Li, D. C.; Yoshitake, H.; Wang, H. Y. Effect of surface modification on electrochemical performance of nano-sized Si as an anode material for Li-ion batteries. *RSC Adv.* **2016**, *6*, 34715-34723.